Pergamon

Geochimica et Cosmochimica Acta, Vol. 63, No. 21, pp. 3567–3578, 1999

0016-7037/99 $20.00 + .00

PII S0016-7037(99)00277-X

The speciation of dissolved water in rhyolitic melt

PHILLIP D. IHINGER,* YOUXUE ZHANG,† and EDWARD M. STOLPER
Division of Geological and Planetary Sciences, California Institute of Technology, Pasadena, CA 91125, USA

(*Received February* 5, 1999; *accepted in revised form June* 21, 1999)

Abstract—Concentrations of water molecules and hydroxyl groups have been measured in rhyolitic glasses with 0.5% to 5.0% H_2O_t using infrared spectroscopy at room temperature. The glasses were cooled at $\sim 10^2$C/s after having been held at 400 to 600C, for sufficient time for the equilibrium distribution of species to have been reached. The speciation of water in samples with greater than 2.5 wt.% total dissolved water and quenched rapidly from temperatures ≥600C were shown to reequilibrate during quench. However, samples with less than 2.0% water and quenched rapidly from ≤600C, and those with less than 5.5% water and quenched rapidly from ≤500C, did not undergo changes on quench and record the equilibrium species concentrations of the experimental run conditions. Knowledge of the equilibrium speciation of water in samples at lower temperatures can be used to predict the species concentrations at magmatic temperatures and allow us to explore the effect of melt structure on the physical properties of natural hydrous magmas. Ideal mixing models can be used as a rough approximation for modeling the solution of water in rhyolitic melts with less than 2.5 wt.% total water:

$$\ln[(X_{\mathrm{OH}}^{\mathrm{melt}})^2/(X_{\mathrm{H_2O}_m}^{\mathrm{melt}} X_{\mathrm{O}}^{\mathrm{melt}})] = \ln\ K = 1.89 \pm 0.05 - (3120 \pm 40)/T,$$

where X_i^{melt} is the mole fraction of species i on a single oxygen basis, H_2O_m = water molecules, O = anhydrous oxygens, and T is temperature in Kelvin. This fit provides a standard state enthalpy and entropy of $\Delta H^\circ = 25.9 \pm 0.4$ kJ/mol and $\Delta S^\circ = 15.7 \pm 0.4$ J/mol · K for the mixing of water molecules in rhyolitic melt. At high water contents, either a modification to the infrared calibration or more complex models (such as a regular solution model) are required to fit the data.

Our measurements differ with recent studies using in situ measurement techniques that show lesser concentrations of molecular species at magmatic temperatures, and we address concerns associated with the in situ method. Our study on quenched glasses can be applied to natural rhyolites; using measured species concentrations, the "apparent" equilibration temperature can be calculated to within 12°C (2σ uncertainty) which can be used to determine the cooling rate of a naturally quenched rhyolitic glass. *Copyright © 1999 Elsevier Science Ltd*

1. INTRODUCTION

The nature of water dissolved in silicate melt has received considerable attention from geologists for many years (e.g., Goranson, 1938; Wasserburg, 1957; Burnham, 1975; Stolper, 1982a; b). It is well known that the structure of a silicate melt is altered with the dissolution of water such that the addition of small amounts of water can significantly change its physical and chemical properties. The presence of water in a magmatic system influences, for example, the liquidus and solidus temperatures (e.g., Tuttle and Bowen, 1958; Kushiro, 1969; Wyllie, 1979), the viscosity of the liquid (e.g., Shaw, 1963; Burnham, 1967; Dingwell et al., 1996; Schulze et al., 1996; Stevenson et al., 1998), crystal nucleation rates (Davis et al., 1997), and the chemical diffusivities that control melt homogenization, crystal growth rates, and the degree of interaction with surrounding wall-rock (e.g., Watson, 1979; Zhang et al., 1991). It is generally accepted that in felsic liquids these effects are related to reactions that form hydroxyl groups (hereafter referred to as OH) from dissolved H_2O molecules (hereafter referred as H_2O_m; the total dissolved H_2O content, i.e., the sum of the amounts of water dissolved as OH and H_2O_m, will be referred to as H_2O_t) and tetrahedral aluminosilicate units in the melt. However, neither the details of these reactions (Mysen and Virgo, 1986; Kohn et al., 1989; McMillan et al., 1992; Sykes and Kubicki, 1993), nor the abundances of OH and H_2O_m in felsic liquids and glasses (including their dependences on H_2O_t and temperature; Stolper, 1989; Dingwell and Webb, 1990; Mysen, 1993; Nowak and Behrens, 1995; Shen and Keppler, 1995; Romano et al., 1995; Behrens and Nowak, 1997) are fully agreed upon or understood.

This paper presents experimental results on the dependence of the speciation of water in felsic melts and glasses on temperature and H_2O_t. Some of the results presented in this study (especially speciation at low H_2O_t) have been utilized in other studies that have focused on other aspects of the interaction of water with silicate melt (Ihinger, 1991; Zhang et al., 1991; 1995; 1997). The data base reported here combines data used in these studies with new experimental data and spans the entire range of temperature and dissolved water content accessible to our experimental technique. We present in this paper a formal treatment of the speciation of water in silicate melts as deduced from measurements made on quenched glasses at room temperature, and we discuss some caveats regarding interpretation of in situ infrared (IR) measurements of speciation made on

* Address reprint requests to Phillip D. Ihinger, Department of Geology and Geophysics, Yale University, New Haven, CT 06520-8109, USA.
† *Present address:* Dept. of Geological Sciences, The University of Michigan, Ann Arbor, MI 48109-1063, USA.

Table 1. Starting material compositions.

	Mono Craters[a]	GB	LPR1	LPR2	LPR3	Q3	Q8
SiO_2	76.4	77.6	76.6	76.6	76.6	74.2	72.6
Al_2O_3	12.3	12.9	12.7	12.7	12.7	12.4	12.1
FeO	1.0	0.4	2.2	2.2	2.2	0.0	0.7
CaO	0.5	0.5	0.3	0.3	0.3	0.0	0.7
Na_2O	3.8	4.2	4.1	4.1	4.1	4.0	3.5
K_2O	4.8	4.2	4.6	4.6	4.6	4.8	4.7
H_2O_t	variable	variable	3.5	4.8	4.0	3.2	3.1
Notes	[b]	[c]	[d]	[e]	[e]		
Synthesis conditions							
T(C)	—	850	850	850	850	1300	1100
P (bar)	—	500	550	1100	700	1000	1000
Time (h)	—	500	140	118	125	20	65
Apparatus[f]	—	CSPV	IHPV	IHPV	IHPV	IHPV	IHPV

[a] All values reported as wt.%.
[b] Samples collected by Sieh and Bursik (1986). Microprobe analyses represent average of 15 samples (Newman et al., 1988). See Table 2 for total water contents.
[c] Obsidian from Glass Buttes, Oregon collected by Ihinger (1991).
[d] Obsidian from Los Pasos, New Mexico; analysis from Shaw (1963) on prehydrated sample. Water content determined by IR from Stanton (1989).
[e] Synthesized by Hamilton from oxide powders plus excess water sealed in Pt capsules. Microprobe analyses represent average of ten spots on hydrated samples.
[f] CSPV = cold-seal pressure vessels; IHPV = internally heated pressure vessels.

samples at magmatic pressures and temperatures (Nowak and Behrens, 1995; Shen and Keppler, 1995).

In this study, hydrous rhyolitic melts and glasses were held under run conditions for sufficient time to approach an equilibrium distribution of species and then quenched to room temperature on time scales short enough that the high-temperature distributions of hydrous melt species were preserved in the quenched glasses. Species concentrations measured by Fourier transform infrared (FTIR) spectroscopy at room temperature on these quenched glasses thus provide quantitative constraints on speciation at high temperatures. This approach to characterizing the temperature dependence of the speciation of water in rhyolitic glasses was first used by Stolper (1989), in which samples were quenched from temperatures ranging from 300 to 900C. At about the same time the quenchability of water speciation was questioned by Dingwell and Webb (1990) who outlined a qualitative prediction of quenchability based on viscosity. Here, we confirm that samples with high water contents quenched from high temperatures can change their speciation on quench. There is, however, a restricted range of temperatures and water contents for a given quench rate that allow for the preservation of the equilibrium species concentrations at run temperature. Using samples quenched from conditions that satisfy criteria for species preservation, we constrain a thermodynamic model of the equilibrium speciation of water in rhyolite as a function of temperature and H_2O_t. This model provides a description of the relative abundances of H_2O_m and OH under magmatic conditions that can be used in determining the effect of water on melt properties such as viscosity and cation diffusivity and on magmatic processes such as rates of assimilation, mixing, bubble growth, and crystal nucleation and growth.

2. EXPERIMENTAL METHODS

Natural and synthetic rhyolitic glasses were held at 400 to 600°C for 40 s to 50 days, at pressures of ~1 to 1000 bar. The concentrations of hydrous species in each glass were determined by FTIR spectroscopy before and after each experiment.

2.1. Starting Materials

Chemical compositions of all starting materials are listed in Table 1. Rhyolitic obsidians with 0.45 to 2.3 wt.% (wt.% is shortened to % hereafter) H_2O_t from the Mono Craters, California were used as starting materials in the 1 atm experiments. These glasses have been described by Sieh and Bursik (1986), Newman et al. (1986; 1988) and Zhang et al. (1991). One high-pressure experiment (PD-D2 in Table 2) at 250 bar also used a natural obsidian as the starting material. Starting materials for all other high-pressure experiments were synthesized. Sample GB was synthesized by hydrating rhyolitic obsidian from Glass Buttes, Oregon in our laboratory. LPR samples were synthesized by Dr. T. Stanton at the Arizona State University (Stanton, 1989) by hydrating rhyolitic obsidian from Los Pasos, New Mexico. Samples Q3 and Q8 were prepared by Dr. D. Hamilton at the University of Manchester (UK). Synthesis conditions for all these starting materials are given in Table 1. All starting materials were aphyric except for the presence of opaque oxides (<5 μm) and rare feldspar grains (<100 μm) in some natural obsidians.

2.2. Equilibration Experiments

One atm experiments were described in detail by Zhang et al. (1991, 1995) and are only summarized here. Doubly polished glass wafers (2–10 mm wide and long by 0.36–3.4 mm thick) were held at elevated temperature in 1 atm tube furnaces for 40 s to 50 days under flowing N_2 such that hydrous species concentrations reequilibrated to the new conditions before loss of water by diffusion significantly altered H_2O_t. Temperatures were controlled with a chromel–alumel thermocouple outside the tube and monitored with a chromel–alumel thermocouple adjacent to the experimental charge. Glass wafers were quenched by pulling them out of the furnace and dropping them into water. As noted in Table 2, some of the samples from the 1-atm experiments (particularly those with high H_2O_t) experienced bubble formation, deformation, and discoloration. However, as discussed by Zhang et al. (1991), these changes do not appear to affect measured species concentrations.

Because samples with high H_2O_t ($\geq$2.5%) deform and bubble during heating at 1 atm, experiments to determine species equilibrium for such samples were conducted at high pressures (up to 1000 bar) in vertical rapid-quench, cold-seal pressure vessels as described in Ihinger (1991). For each experiment, starting materials (doubly polished, ~3 × 3 ×

0.3 3-mm chips with homogeneous H_2O_m and OH contents) were sealed in Pt capsules. The capsules were pressurized in the cold part of a pressure vessel to 250 to 1000 bar using distilled water as the pressurizing medium and then levitated magnetically within the pressure vessel into the hot zone of the furnace. The pressure was chosen to be greater than the vapor saturation pressure of the samples (based on H_2O_t) so as to prevent bubble formation. Temperatures were monitored with external chromel–alumel thermocouples previously shown to be 13 ± 3C cooler than the internal hot spot (Ihinger, 1991). Quenches were achieved by removing the magnetic levitation and allowing the sample to fall to a cold part of the pressure vessel. The time scales for quenching in these experiments (and in the 1-atm experiments) depended on the thermal diffusivity and the thickness of the sample and were on the order of 1 s ($\sim 10^2$C/s). After quenching, some samples from the high-pressure experiments exhibited a dull "frosting"; these samples were repolished with 1 μm alumina to remove the "frost" before FTIR analysis. No bubbles or other changes relative to the starting materials were observed in the polished, high-pressure run products.

2.3. Infrared Spectroscopy

All starting materials and run products were analyzed for H_2O_m and OH using an FTIR Nicolet 60SX spectrometer following the procedures of Newman et al. (1986). Apertures used to delimit the infrared beam depended on sample size and heterogeneity; i.e., smaller apertures or narrower slits were used for smaller and more heterogeneous samples. The intensities (peak heights) of the absorption bands at 5230 cm^{-1} (A_{5230}) and 4520 cm^{-1} (A_{4520}) were measured. The baseline is fit by a flexicurve. Uncertainties on the infrared spectroscopic measurements have been estimated based on the quality of individual spectra, the reproducibility of an internal standard analyzed repeatedly along with the unknowns, and the reproducibility of analyses of different polished sections of the same sample. Precisions for single measurements of A_{5230} and A_{4520} were taken as the larger of ±1% relative or ±0.001 absolute absorbance units (all the precisions stated and error bars shown in this paper are at the $\pm 2\sigma$ level).

Species concentrations were calculated using the molar absorptivites from Zhang et al. (1997). The concentrations (in wt.%) of OH and H_2O_m are calculated using the following relations:

$$H_2O_m = \delta_{5230} A_{5230}; \quad (1)$$

$$OH = \delta_{4520} A_{4520}; \quad (2)$$

where

$$\delta_{5230} = (\rho/18.015)(a_0); \quad (3)$$

$$\delta_{4520} = (\rho/18.015)(b_0 - b_1 A_{5230} + b_2 A_{4520}); \quad (4)$$

and

$$\rho/\rho_0 H_2O_t = \delta_{5230} A_{5230} + \delta_{4520} A_{4520}; \quad (5)$$

where ρ is glass density, ρ_0 is the density of anhydrous glass of an otherwise identical composition, $a_0 = 0.04217$, $b_0 = 0.04024$, $b_1 = 0.02011$, and $b_2 = 0.0522$. Eqn. 2 represents a modified Beer–Lambert relationship in that the molar absorptivity, $1/\delta_{4520}$, is dependent on H_2O_m as well as OH. The dependence of glass density on H_2O_t is expressed as $\rho/\rho_0 \sim 1 - H_2O_t/100$. As Zhang et al. (1997) assessed, the above calibration for species concentrations is best constrained for $H_2O_t \leq 2.7\%$, although the applicability for H_2O_t content is up to 5.5% H_2O_t.

Following Zhang et al. (1995), we use the parameter

$$Q \equiv \frac{(X_{OH}^{glass})^2}{X_{H_2O_m}^{glass} X_O^{glass}} \quad (6)$$

to describe the proportions of OH and H_2O_m in a sample, where X_i^{glass} is the measured mole fraction of species i in the glass on a single oxygen basis, and O denotes an anhydrous oxygen (Stolper, 1982b). Propagated errors on Q are typically ~2% relative except when A_{5230} and/or A_{4520} are less than 0.1 (e.g., for thin samples or samples with low H_2O_t). Analyses of different spots in the same sample sometimes have uncertainties in individual species concentrations larger than 1% due to heterogeneity. However, even for these samples, the precision for Q based on multiple spectra from different spots is usually less than or equal to the typical value of 2% relative error, due to correlated variations in $X_{H_2O_m}$ and X_{OH}.

3. RESULTS AND DISCUSSION

The concentrations of H_2O_m and OH in all quenched glasses are listed in Table 2. The actual IR absorbance data are also reported because there may be further improvement in the IR calibration. Both the 1-atm and the high-pressure data are used to examine the dependence of speciation on temperature and H_2O_t because the effect of pressure is negligible for pressures less than 1 kbar (Zhang, 1993). The equilibrium constants are plotted as a function of H_2O_t and $1/T$ in Figure 1.

3.1. Melt Species Equilibrium and the Effect of Quench

In order to demonstrate that our measurements represent equilibrium distributions of hydrous species at run conditions, we must show that (1) samples have attained equilibrium during the duration of the run, and (2) samples have not undergone changes in species concentrations during the quench to room temperature.

Attainment of equilibrium for some experiments (Zhang et al., 1995) has been demonstrated by "reversals" (i.e., approaching a final value of Q from initially higher and lower values) or by observing that Q no longer varies with heating duration. The degree to which an equilibrium distribution of species was achieved in other experiments has been evaluated by comparison of run durations with time scales for equilibrium determined by Zhang et al. (1995). Specifically, the durations of all 1-atm equilibrium speciation experiments reported here are greater than or equal to the time required to reach equilibrium ($\sim 5\tau_r$ as given in Fig. 3 of Zhang et al., 1995). At low temperatures (400–480C), the durations of the 1-atm experiments were all significantly longer than the estimated times to reach equilibrium based on extrapolation of the results of Zhang et al. (1995). For the high-pressure experiments, run durations were at least twice ($10\tau_r$) the time calculated as necessary to reach equilibrium.

Zhang et al. (1991, 1995) discussed the conditions under which concentrations of hydrous species can be preserved on quenching of rhyolitic glasses; i.e., conditions for which the back reaction for $H_2O_m + O = 2\ OH$ is negligible. They showed that for samples quenched at a given rate, the quench effect can be neglected only for samples with less than a particular critical concentration of H_2O_t, where the critical concentration is inversely correlated with the temperature of the experiment. For example, for a quench rate of ~200C/s, the quench effect can be neglected for samples with $H_2O_t \lesssim 2.0\%$ quenched from 600C, for samples with $\lesssim 3.2\%$ quenched from 550C, and with $\lesssim 5.5\%$ for samples quenched from 500C. Only those samples that satisfy these conditions are included in the equilibrium data base (the upper part of Table 2). The lower part of Table 2 includes experimental data from this study that are not used to constrain equilibrium speciation for rhyolitic glasses and melts. For example, based on the analysis in Zhang et al. (1991, 1995), some samples (e.g., with >3% H_2O_t at 600C) underwent significant species reequilibration upon

Table 2. The equilibrium speciation of water in rhyolite. Water contents determined using species-dependent molar absorptivities from Zhang et al. (1997) as described in text.

					Band intensities															
Sample	Temp (C)	Pressure (bar)	Time	1000/T	Error 2σ	5230 abs	Error 2σ	4520 abs	Error 2σ	Thickness (mm)	Density (kg/m^3)	H_2O_m (wt.%)	OH (wt.%)	H_2O_t (wt.%)	$X(H_2O_t)$	$X(H_2O_m)$	X(OH)	X(O)	ln K	Comments error
Mn85-D4.042	600	1	10 min	1.14528	0.0065	0.0896	0.0010	0.3240	0.0032	2.43	2344	0.157	0.624	0.781	0.014	0.003	0.022	0.975	−1.699	0.02 k
POB1-D2A.041	600	1	10 min	1.14528	0.0065	0.1500	0.0015	0.4980	0.0050	3.42	2343	0.187	0.690	0.876	0.016	0.003	0.025	0.972	−1.671	0.02 k
POB10-D1c.031	600	1	6 min	1.14528	0.0065	0.2050	0.0021	0.5530	0.0055	3.3	2340	0.265	0.809	1.073	0.019	0.005	0.029	0.966	−1.700	0.02 k
POB10-D1C.041	600	1	10 min	1.14528	0.0065	0.2040	0.0020	0.5525	0.0055	3.3	2340	0.264	0.808	1.071	0.019	0.005	0.029	0.966	−1.697	0.02 k
MC84.421	600	1002	20 min	1.14528	0.0130	0.0137	0.0010	0.0312	0.0003	0.16	2337	0.365	0.961	1.325	0.024	0.007	0.034	0.959	−1.670	0.08 hp
3b-D6A.111	600	1	120 s	1.14528	0.0065	0.1695	0.0017	0.3590	0.0036	1.737	2335	0.418	1.029	1.447	0.026	0.007	0.037	0.956	−1.665	0.02 k
3b-D6A.112	600	1	120 s	1.14528	0.0065	0.1775	0.0018	0.3630	0.0036	1.742	2335	0.436	1.038	1.474	0.026	0.008	0.037	0.955	−1.691	0.02 k
3b-D5dif.051	550	1	13.8 d	1.21485	0.0073	0.0170	0.0010	0.0870	0.0010	1.035	2348	0.070	0.374	0.444	0.008	0.001	0.013	0.985	−1.919	0.06 d
3b-D5dif.052	550	1	13.8 d	1.21485	0.0073	0.0168	0.0010	0.0858	0.0010	1.035	2349	0.069	0.368	0.437	0.008	0.001	0.013	0.986	−1.935	0.06 d
KS-D4B.091A	550	1	12 min	1.21485	0.0073	0.0825	0.0010	0.2440	0.0024	1.841	2344	0.191	0.618	0.809	0.014	0.003	0.022	0.974	−1.914	0.02 k
KS-D4B.092	550	1	12 min	1.21485	0.0073	0.0750	0.0010	0.2330	0.0023	1.826	2344	0.175	0.592	0.767	0.014	0.003	0.021	0.976	−1.912	0.02 k
KS-D4B.101A	550	1	22 min	1.21485	0.0073	0.0800	0.0010	0.2415	0.0024	1.84	2344	0.185	0.611	0.796	0.014	0.003	0.022	0.975	−1.905	0.02 k
KS-D4B.102	550	1	22 min	1.21485	0.0073	0.0740	0.0010	0.2330	0.0023	1.83	2344	0.172	0.591	0.763	0.014	0.003	0.021	0.976	−1.901	0.02 k
KS-D5.051	550	1	13.8 d	1.21485	0.0073	0.0805	0.0010	0.2435	0.0024	1.832	2344	0.187	0.620	0.807	0.014	0.003	0.022	0.974	−1.887	0.02 d
KS-D5.052	550	1	13.8 d	1.21485	0.0073	0.0840	0.0010	0.2475	0.0025	1.821	2343	0.196	0.636	0.832	0.015	0.004	0.023	0.974	−1.885	0.02 d
POB1-D1.051	550	1	13.8 d	1.21485	0.0073	0.0805	0.0010	0.2370	0.0024	1.7	2343	0.201	0.655	0.856	0.015	0.004	0.023	0.973	−1.853	0.02 d
3b-D1B1.121	550	1	4 min	1.21485	0.0073	0.1260	0.0013	0.2450	0.0025	1.314	2337	0.410	0.908	1.318	0.024	0.007	0.032	0.960	−1.901	0.02 k
3b-D1B1.131	550	1	10 min	1.21485	0.0073	0.1245	0.0012	0.2440	0.0024	1.314	2337	0.405	0.904	1.309	0.023	0.007	0.032	0.961	−1.898	0.02 k
3b-D1B2.121	550	1	4 min	1.21485	0.0073	0.1300	0.0013	0.2500	0.0025	1.32	2336	0.421	0.924	1.345	0.0024	0.008	0.033	0.960	−1.891	0.02 k
3b-D1B2.122	550	1	4 min	1.21485	0.0073	0.1265	0.0013	0.2470	0.0025	1.32	2337	0.410	0.912	1.321	0.024	0.007	0.033	0.960	−1.891	0.02 k
3b-D1B2.131	550	1	10 min	1.21485	0.0073	0.1275	0.0013	0.2480	0.0025	1.32	2337	0.413	0.916	1.329	0.024	0.007	0.033	0.960	−1.890	0.02 k
3b-D6A.061	550	1	3 min	1.21485	0.0073	0.1980	0.0020	0.3460	0.0035	1.744	2335	0.486	0.973	1.459	0.026	0.009	0.035	0.957	−1.930	0.02 k
3b-D6A.071	550	1	4 min	1.21485	0.0073	0.1980	0.0020	0.3480	0.0035	1.739	2335	0.487	0.983	1.470	0.026	0.009	0.035	0.956	−1.912	0.02 k
3b-D6A.081	550	1	7.5 min	1.21485	0.0073	0.1980	0.0020	0.3450	0.0035	1.736	2335	0.488	0.975	1.463	0.026	0.009	0.035	0.957	−1.931	0.02 k
3a-D2C.031	550	1	90 s	1.21485	0.0073	0.1896	0.0019	0.2274	0.0023	0.838	2323	0.977	1.386	2.363	0.042	0.017	0.049	0.934	−1.904	0.02 k
3a-D2C.032	550	1	90 s	1.21485	0.0073	0.1884	0.0019	0.2244	0.0022	0.84	2324	0.968	1.359	2.327	0.041	0.017	0.048	0.935	−1.935	0.02 k
3a-D2C.033	550	1	90 s	1.21485	0.0073	0.1872	0.0019	0.2250	0.0023	0.84	2324	0.962	1.364	2.326	0.041	0.017	0.048	0.935	−1.921	0.02 k
KS-big.101P	540	1	302 min	1.22979	0.0075	0.0420	0.0010	0.1218	0.0012	0.903	2343	0.198	0.630	0.828	0.015	0.004	0.023	0.974	−1.912	0.03 k
KS-big.102P	540	1	302 min	1.22979	0.0075	0.0423	0.0010	0.1215	0.0012	0.903	2343	0.199	0.628	0.828	0.015	0.004	0.023	0.974	−1.925	0.03 k
KS-big.103P	540	1	302 min	1.22979	0.0075	0.0438	0.0010	0.1242	0.0012	0.903	2343	0.206	0.644	0.851	0.015	0.004	0.023	0.973	−1.910	0.03 k
KS-big.104P	540	1	302 min	1.22979	0.0075	0.0420	0.0010	0.1215	0.0012	0.903	2343	0.198	0.629	0.826	0.015	0.004	0.023	0.974	−1.917	0.03 k
KS-D2.051	530	1	11.4 d	1.24510	0.0077	0.0290	0.0010	0.0800	0.0010	0.593	2343	0.208	0.630	0.838	0.015	0.004	0.023	0.974	−1.963	0.04 d
KS-D2.052	530	1	11.4 d	1.24510	0.0077	0.0292	0.0010	0.0802	0.0010	0.593	2343	0.209	0.632	0.841	0.015	0.004	0.023	0.974	−1.965	0.04 d
KS-D2.061	530	1	11.4 d	1.24510	0.0077	0.0296	0.0010	0.0794	0.0010	0.593	2343	0.212	0.624	0.836	0.015	0.004	0.022	0.974	−2.002	0.04 d
3b-D3.051	530	1	11.4 d	1.24510	0.0077	0.0302	0.0010	0.0620	0.0010	0.37	2339	0.348	0.802	1.149	0.021	0.006	0.029	0.965	−1.988	0.05 d
3b-D3.101	530	1	11.4 d	1.24510	0.0077	0.0299	0.0010	0.0614	0.0010	0.365	2339	0.349	0.805	1.154	0.021	0.006	0.029	0.965	−1.982	0.05 d
3b-D3.102	530	1	11.4 d	1.24510	0.0077	0.0294	0.0010	0.0603	0.0010	0.365	2339	0.344	0.789	1.133	0.020	0.006	0.028	0.966	−2.008	0.05 d
3b-D3.105	530	1	11.4 d	1.24510	0.0077	0.0305	0.0010	0.0610	0.0010	0.365	2339	0.356	0.799	1.155	0.021	0.006	0.029	0.965	−2.017	0.05 d
LPR1.111e	530	744	10 min	1.24510	0.0153	0.5768	0.0058	0.4304	0.0043	1.249	2305	2.024	1.753	3.777	0.066	0.035	0.061	0.903	−2.140	0.02 hp
LPR2.111	530	744	10 min	1.24510	0.0153	0.7380	0.0074	0.4650	0.0047	1.258	2296	2.589	1.846	4.435	0.077	0.045	0.064	0.891	−2.273	0.02 hp
LPR3.111	530	744	10 min	1.24510	0.0153	0.6544	0.0065	0.4504	0.0045	1.266	2301	2.272	1.796	4.068	0.071	0.040	0.063	0.898	−2.203	0.02 hp
LPR3.112	530	744	10 min	1.24510	0.0153	0.6504	0.0065	0.4488	0.0045	1.261	2301	2.267	1.797	4.064	0.071	0.040	0.063	0.898	−2.199	0.02 hp
6b1-D1.061	500	1	110 min	1.29341	0.0083	0.1510	0.0015	0.3380	0.0034	2.4	2342	0.268	0.659	0.926	0.017	0.005	0.024	0.972	−2.126	0.02 k
6b1-D2.061	500	1	110 min	1.29341	0.0083	0.1720	0.0017	0.3585	0.0036	2.415	2341	0.303	0.698	1.001	0.018	0.005	0.025	0.970	−2.132	0.02 k
POB10-D2A.061	500	1	110 min	1.29341	0.0083	0.2260	0.0023	0.4460	0.0045	2.907	2340	0.331	0.724	1.055	0.019	0.006	0.026	0.968	−2.147	0.02 k
3b-D1B.041P	500	1	50 min	1.29341	0.0083	0.1462	0.0015	0.2400	0.0024	1.318	2336	0.474	0.877	1.351	0.024	0.008	0.031	0.960	−2.116	0.02 k
3b-D1B.042P	500	1	50 min	1.29341	0.0083	0.1420	0.0014	0.2365	0.0024	1.314	2337	0.462	0.866	1.328	0.024	0.008	0.031	0.961	−2.116	0.02 k

(Continued)

Table 2. (Continued)

3b-D1B.043P	500	1	50 min	1.29341	0.0083	0.1402	0.0014	0.2340	0.0023	1.3	2337	0.461	0.866	1.327	0.024	0.008	0.031	0.961	−2.113	0.02 k
3b-D1B.061	500	1	110 min	1.29341	0.0083	0.1445	0.0014	0.2380	0.0024	1.315	2337	0.470	0.871	1.341	0.024	0.008	0.031	0.961	−2.120	0.02 k
3b-D1B1.001	500	1	110 min	1.29341	0.0083	0.1390	0.0014	0.2345	0.0023	1.316	2337	0.451	0.856	1.307	0.023	0.008	0.031	0.961	−2.115	0.02 k
3b-D1B2.001	500	1	110 min	1.29341	0.0083	0.1440	0.0014	0.2375	0.0024	1.316	2337	0.468	0.868	1.336	0.024	0.008	0.031	0.961	−2.123	0.02 k
3b-D1B3.001	500	1	110 min	1.29341	0.0083	0.1043	0.0010	0.1745	0.0017	0.971	2337	0.459	0.864	1.323	0.024	0.008	0.031	0.961	−2.113	0.02 k
3b-D1B4.001	500	1	110 min	1.29341	0.0083	0.1035	0.0010	0.1733	0.0017	0.975	2337	0.454	0.853	1.307	0.023	0.008	0.030	0.961	−2.127	0.02 k
MC84.211	500	994	60 min	1.29341	0.0165	0.0819	0.0010	0.1340	0.0013	0.733	2336	0.478	0.881	1.358	0.024	0.009	0.031	0.960	−2.115	0.02 hp
GB45.211	500	994	60 min	1.29341	0.0165	0.0833	0.0010	0.0811	0.0010	0.288	2319	1.253	1.421	2.674	0.047	0.022	0.050	0.928	−2.098	0.03 hp
LPR1.411	500	994	60 min	1.29341	0.0165	0.3079	0.0031	0.2237	0.0022	0.675	2306	1.997	1.664	3.661	0.064	0.035	0.058	0.907	−2.233	0.02 hp
LPR2.411	500	994	60 min	1.29341	0.0165	0.3660	0.0037	0.2148	0.0021	0.594	2296	2.720	1.769	4.490	0.078	0.047	0.062	0.891	−2.409	0.02 hp
LPR3.411	500	994	60 min	1.29341	0.0165	0.3218	0.0032	0.2203	0.0022	0.636	2303	2.222	1.737	3.959	0.069	0.039	0.061	0.900	−2.250	0.02 hp
KS-D3.101	490	1	18.6 d	1.31036	0.0085	0.0660	0.0010	0.1605	0.0016	1.257	2344	0.223	0.590	0.813	0.015	0.004	0.021	0.975	−2.165	0.03 d
POB10-D3.101	490	1	18.6 d	1.31036	0.0085	0.1365	0.0014	0.2580	0.0026	1.668	2340	0.349	0.730	1.079	0.019	0.006	0.026	0.968	−2.182	0.02 d
POB10-D3.102	490	1	18.6 d	1.31036	0.0085	0.1415	0.0014	0.2600	0.0026	1.67	2340	0.361	0.735	1.096	0.020	0.006	0.026	0.967	−2.204	0.02 d
3b-D1.101	490	1	18.6 d	1.31036	0.0085	0.1750	0.0018	0.2760	0.0028	1.566	2337	0.478	0.843	1.320	0.024	0.009	0.030	0.961	−2.203	0.02 d
3b-D1.102	490	1	18.6 d	1.31036	0.0085	0.1765	0.0018	0.2740	0.0027	1.566	2337	0.482	0.835	1.317	0.024	0.009	0.030	0.962	−2.230	0.02 d
PD-D2.102	490	250	11 d	1.31036	0.0169	0.2990	0.0030	0.2365	0.0024	0.814	2314	1.598	1.439	3.036	0.053	0.028	0.051	0.921	−2.312	0.02 h
PD-D2.103	490	250	11 d	1.31036	0.0169	0.2844	0.0028	0.2316	0.0023	0.8	2315	1.545	1.438	2.984	0.053	0.027	0.051	0.922	−2.280	0.02 h
PD-D2.104	490	250	11 d	1.31036	0.0169	0.3018	0.0030	0.2364	0.0024	0.814	2314	1.613	1.436	3.049	0.054	0.028	0.051	0.921	−2.325	0.02 h
PD-D2.110	490	250	11 d	1.31036	0.0169	0.2010	0.0020	0.2060	0.0021	0.825	2324	1.051	1.236	2.288	0.041	0.019	0.044	0.938	−2.209	0.02 h
PD-D2.111	490	250	11 d	1.31036	0.0169	0.1512	0.0015	0.1795	0.0018	0.826	2330	0.786	1.061	1.847	0.033	0.014	0.038	0.948	−2.233	0.02 h
MC84.311	475	1009	10 h	1.33663	0.0176	0.0511	0.0010	0.0747	0.0010	0.422	2336	0.518	0.844	1.362	0.024	0.009	0.030	0.961	−2.281	0.03 h
GB45.311	475	1009	10 h	1.33663	0.0176	0.1178	0.0012	0.1060	0.0011	0.396	2320	1.288	1.325	2.613	0.046	0.023	0.047	0.930	−2.268	0.02 h
Mn85-D1A.051	450	1	51.7 d	1.38284	0.0095	0.0452	0.0010	0.0956	0.0010	0.838	2344	0.229	0.519	0.748	0.013	0.004	0.019	0.977	−2.453	0.03 d
KS-D5A.051	450	1	51.7 d	1.38284	0.0095	0.0800	0.0010	0.1560	0.0016	1.313	2344	0.259	0.542	0.801	0.014	0.005	0.019	0.976	−2.487	0.02 d
KS-D5A.052	450	1	51.7 d	1.38284	0.0095	0.0850	0.0010	0.1603	0.0016	1.313	2343	0.275	0.558	0.833	0.015	0.005	0.020	0.975	−2.488	0.02 d
POB10-D1C.051	450	1	51.7 d	1.38284	0.0095	0.0780	0.0010	0.1194	0.0012	0.8	2340	0.416	0.695	1.111	0.020	0.007	0.025	0.968	−2.454	0.02 d
3b-D1C.051	450	1	51.7 d	1.38284	0.0095	0.0945	0.0010	0.1353	0.0014	0.86	2338	0.469	0.736	1.205	0.022	0.008	0.026	0.965	−2.459	0.02 d
LPR2.211	450	551	130 min	1.38284	0.0189	0.8844	0.0088	0.4296	0.0043	1.258	2293	3.110	1.574	4.684	0.081	0.054	0.055	0.891	−2.779	0.02 h
3b-D4.051	403	1	39.9 d	1.47896	0.0109	0.2170	0.0022	0.2475	0.0025	1.553	2337	0.597	0.739	1.336	0.024	0.011	0.026	0.963	−2.692	0.02 d
3b-D4.052	403	1	39.9 d	1.47896	0.0109	0.2175	0.0022	0.2468	0.0025	1.555	2337	0.598	0.735	1.333	0.024	0.011	0.026	0.963	−2.703	0.02 d
3b-D5.101	403	1	39.9 d	1.47896	0.0109	0.1565	0.0016	0.1470	0.0015	0.783	2331	0.858	0.879	1.737	0.031	0.015	0.031	0.953	−2.699	0.02 d
3a-D2.051	403	1	39.9 d	1.47896	0.0109	0.1007	0.0010	0.0784	0.0010	0.36	2325	1.207	1.024	2.231	0.040	0.021	0.036	0.942	−2.727	0.03 d
The following data may be affected by quenching, may not have reached equilibrium, or is of bulk composition different from natural rhyolite.																			ln Q	
3a-D2C.112	600	1	40 s	1.14528	0.0130	0.1775	0.0018	0.2405	0.0024	0.844	2323	0.909	1.486	2.394	0.042	0.016	0.053	0.931	−1.690	0.02 k, n
3a-D2C.111	600	1	40 s	1.14528	0.0130	0.1703	0.0017	0.2373	0.0024	0.84	2323	0.876	1.473	2.348	0.042	0.015	0.052	0.932	−1.671	0.02 k, n
3a-D2C.101	600	1	20 s	1.14528	0.0130	0.1710	0.0017	0.2350	0.0024	0.84	2324	0.879	1.454	2.333	0.041	0.016	0.051	0.933	−1.701	0.02 k, n
3a-D2C.102	600	1	20 s	1.14528	0.0130	0.1650	0.0017	0.2335	0.0023	0.844	2324	0.844	1.437	2.280	0.040	0.015	0.051	0.934	−1.684	0.02 k, n
GB45.421	600	1002	20 min	1.14528	0.0130	0.0897	0.0010	0.1118	0.0011	0.368	2319	1.056	1.598	2.654	0.047	0.019	0.056	0.925	−1.690	0.02 hp, n
LPR1.231	600	1002	20 min	1.14528	0.0130	0.1248	0.0033	0.1040	0.0033	0.282	2304	1.942	1.941	3.883	0.068	0.034	0.068	0.898	−1.889	0.07 hp, n
LPR2.231	600	1002	20 min	1.14528	0.0130	0.1784	0.0018	0.1121	0.0012	0.287	2293	2.751	1.973	4.724	0.082	0.048	0.069	0.884	−2.196	0.02 hp, n
LPR3.231	600	1002	20 min	1.14528	0.0130	0.1088	0.0011	0.0818	0.0010	0.218	2300	2.196	1.950	4.147	0.072	0.038	0.068	0.894	−2.000	0.03 hp, n
Q3.211	500	994	60 min	1.29341	0.0165	0.2105	0.0021	0.1817	0.0018	0.562	2311	1.633	1.657	3.291	0.058	0.029	0.058	0.913	−2.044	0.02 hp, n, c
Q3.311	475	1009	10 h	1.33663	0.0176	0.2190	0.0022	0.1710	0.0017	0.535	2310	1.787	1.611	3.398	0.060	0.031	0.057	0.912	−2.191	0.02 hp, n, c
Q8.211	500	994	60 min	1.29341	0.0165	0.2645	0.0026	0.2198	0.0022	0.708	2312	1.627	1.570	3.197	0.056	0.029	0.055	0.916	−2.152	0.02 hp, n, c
Q8.421	600	1002	20 min	1.14528	0.0130	0.1546	0.0015	0.1584	0.0016	0.472	2312	1.427	1.774	3.201	0.056	0.025	0.062	0.913	−1.772	0.02 hp, n, c
LPR1.211	450	551	130 min	1.38284	0.0189	0.5872	0.0059	0.3768	0.0038	1.24	2308	2.070	1.467	3.537	0.062	0.036	0.051	0.912	−2.526	0.02 hp, n

[k] Kinetics experiments; [d] Diffusion experiments; [h] Hydration experiments; [hp] High pressure experiments on hydrous glass without adding water; [n] Not included in regression; [c] The major oxide composition is slightly different from the other rhyolitic glasses.

quenching. In addition, samples with H_2O_t only slightly more than those predicted to have quench problems (such as 2%–3% H_2O_t at 600C; see later discussion) have also been excluded from the equilibrium database. The speciation data for starting compositions Q3 and Q8 are believed to represent equilibrium, but are included in the lower part of Table 2 because their major element compositions differ from the natural compositions of the other samples studied.

The temperatures of some of our experiments are lower than what would typically be taken as the "glass transition temperature" based on bulk or macroscopic properties (e.g., viscosity or heat capacity; Dingwell, 1993; Doremus, 1994) under typical laboratory cooling rates. However, in the kinetic definition, the glass transition temperature (or fictive temperature) depends on the cooling rate, and hence the time scale held at a given temperature. As described above, the time scales of our experiments are long enough for the H_2O_m–OH interconversion reactions to reach equilibrium. Therefore, our equilibrium results are representative of relaxed *liquid* rather than unrelaxed *glass* behavior with respect to the reactions controlling interconversion of hydrous species, even though the experiments are at temperatures that might otherwise exhibit a glassy response to thermal or mechanical perturbations experienced on shorter time scales. Note that for those samples that preserve high-temperature speciation on quenching to room temperature, the experimental charge shows what would be called unrelaxed, "glassy" behavior during quenching (Dingwell and Webb, 1990).

3.2. Equilibrium Speciation as a Function of Temperature and H_2O_t

Equilibrium speciation data are listed in Table 2 and results at selected temperatures are plotted in Fig. 1a as ln K (K is defined as Q at equilibrium; see Eqn. 6) vs. H_2O_t for H_2O_t $<2.5\%$ and in Fig. 1b for samples up to 5% H_2O_t. Figure 1a shows that up to ~2.5% H_2O_t, K is independent of water content (within error) at each temperature, indicating that at these concentrations and conditions, the speciation of H-bearing components in these melts can be described by an ideal mixture of H_2O_m, OH, and anhydrous oxygen, as proposed by Stolper (1982b), Silver and Stolper (1985), and Dingwell and Webb (1990). Figure 1c shows ln K vs. $1/T$, with different symbols for different ranges of H_2O_t. The data on samples with less than 2.5% H_2O_t define a single line on this plot; the isotherms on Fig. 1a correspond to points on the best-fit line. The slope of this line indicates a standard state enthalpy change (ΔH°) for the reaction $H_2O_m + O = 2\ OH$ of 25.9 ± 0.3 kJ/mol of H_2O_m, similar to earlier estimates of 25 ± 5 kJ/mol (Dingwell and Webb, 1990) and 23.4 ± 1.0 kJ/mol (Zhang et al., 1991), but smaller than the value base on in situ measurements of species concentrations in peraluminous sodium aluminosilicate with 8.1% H_2O_t (30.3 kJ/mol; Shen and Keppler, 1995), and in haplogranite with 4.14% H_2O_t (33.6 ± 2.0 kJ/mol; Nowak and Behrens, 1995). Figure 2 compares calculated species concentrations using this fit (light solid curves) with measured species concentrations as a function of H_2O_t at 500C and demonstrates that the data up to ~2.5% H_2O_t are fit well by the ideal mixing model, as expected based on the excellent linear fit in Fig. 1c.

While the simple, three-species ideal solution model provides a good approximation, the decrease in K with increasing H_2O_t shown in Fig. 1b for higher H_2O_t is inconsistent with it. One explanation for the apparent nonideality of mixing of hydrous species in silicate melts concerns the accuracy of the calibration of species concentrations at high concentrations of H_2O_t. The calibration of Zhang et al. (1997) was limited to glasses with H_2O_t $<2.7\%$ and may not be applicable to samples with greater water contents. However, we can modify the calibration for δ_{5230} and δ_{4520} in Eqns. 3 and 4 by *assuming* ideal mixing and refitting the results in Table 2 (Zhang and Behrens, 1998). Using the concentration-dependent molar absorptivities, our data yield a best-fit value of $\Delta H^\circ_{\text{ideal}} = 25.3$ kJ/mol, indistinguishable from the value given above for an ideal fit to lower water content glasses.

A second possible explanation for the decrease in K with increasing H_2O_t shown in Fig. 1b for samples with high H_2O_t is that a greater level of complexity (i.e., more free or adjustable model parameters) is required to describe homogeneous equilibria among hydrous species in rhyolitic melts and glasses. This is not surprising because ideality typically only holds for dilute solutions. There are several plausible extensions of the ideal model that can account for the apparent deviation from ideality at high water content (e.g., the formulation of Silver and Stolper, 1989). For example, if we assume that hydroxyl groups are preferentially associated with Al ions (i.e., as AlOH groups; e.g., Sykes and Kubicki, 1993) and consider ideal mixing of $H_2O_m^{melt}$, $AlOSi^{melt}$, $SiOSi^{melt}$, and $AlOH^{melt}$ groups, the deviations from horizontal isotherms shown in Fig. 1b can be modeled. Similarly, an exchange mechanism similar to that of Kohn et al. (1992) modeled as an ideal mixture of $H_2O_m^{melt}$, $(Na, K)OH^{melt}$, $(Al, Si)OH^{melt}$, and $(Na, K)O(Si, Al)^{melt}$ species can also explain these trends. There are other choices and combinations of ideally mixing melt species that could explain our data, and future work will undoubtedly determine the nature of the H-bearing and oxygen-bearing species and the interactions between them. It is important to emphasize that our technique can precisely distinguish H_2O_m and hydroxyl species but not the "subspeciation" at the next detailed level, and this subspeciation may be the key to understanding the variation of K with H_2O_t.

In the absence of a detailed understanding of subspeciation and an unambiguous calibration of the molar absorptivities for high water-content samples, the simplest approximation beyond ideal mixing of H_2O_m, OH, and O in hydrous silicate melt is a regular solution model for mixing of these same idealized species (Silver and Stolper, 1989; Stolper, 1989; Silver et al., 1990; Zhang et al., 1991). For a regular solution of these three melt species, equilibrium is described by the following equation (Silver et al., 1990; Zhang et al., 1991):

$$-\ln K = -\ln\left(\frac{X_{OH}^2}{X_{H_2O_m}X_O}\right) = A + \frac{1000}{T}\left(B + CX_{H_2O_m} + DX_{OH}\right), \quad (7)$$

where A, B, C, and D are constants related to the binary interaction parameters (Ws) among the three melt species (Silver et al., 1990), $1000BR$ (R is the gas constant) is the standard

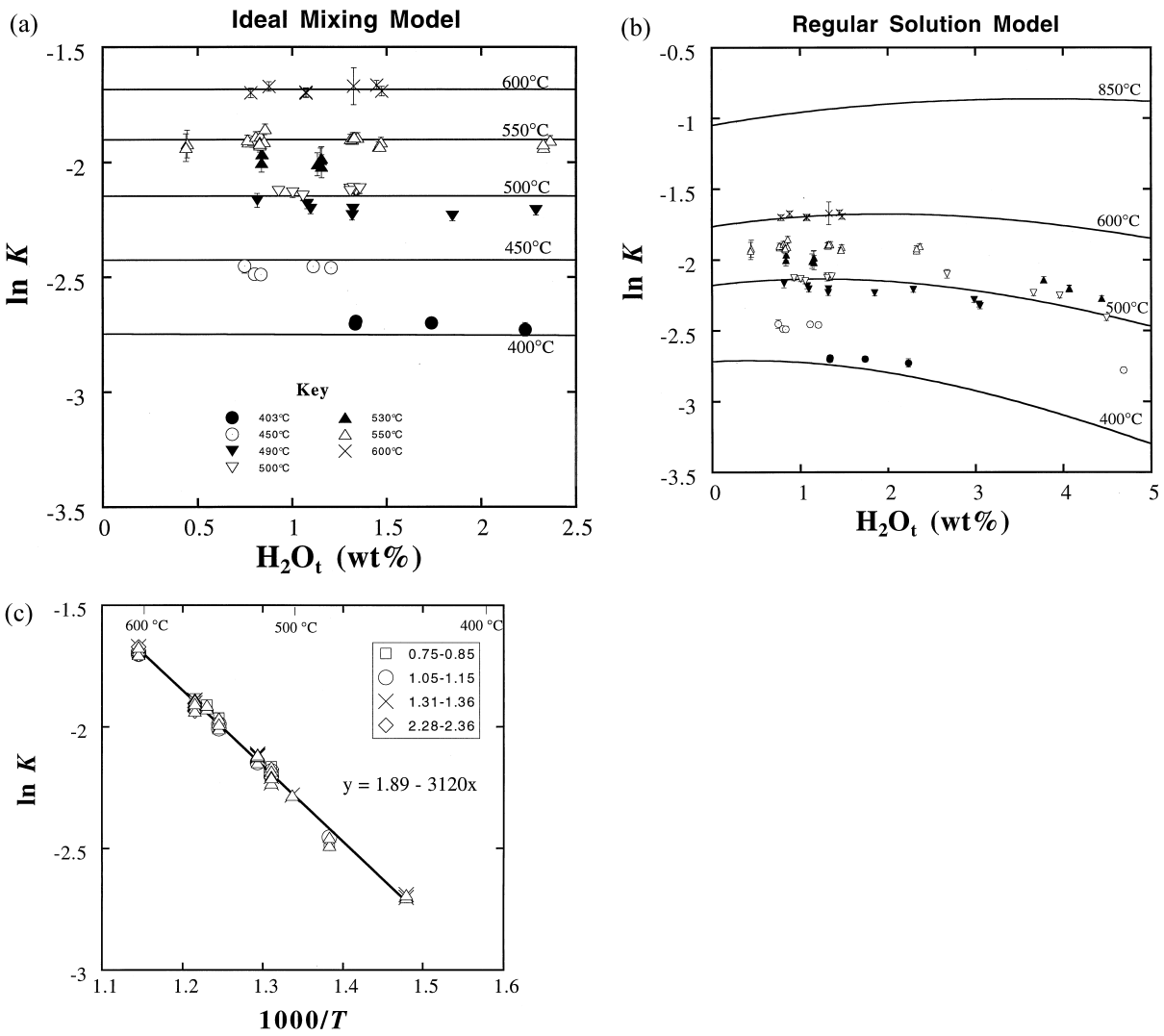

Fig. 1. (a) The dependence of ln K on H_2O_t in rhyolitic samples equilibrated at 400 to 600C with $H_2O_t < 2.5\%$. Only data judged (see text for criteria) to have achieved an equilibrium distribution of species at high temperature and then to have preserved it on quenching are shown. The experimental data with $\pm 2\sigma$ error bars and the best-fit horizontal isotherms based on the ideal mixing model described in the text are shown. For clarity, data at 475 and 540C are not shown. (b) The dependence of ln K on H_2O_t in rhyolitic samples equilibrated at 400 to 600C for samples with $H_2O_t < 5\%$. The experimental data (symbols as in (a)) with 2σ error bars and the best-fit isotherms based on the regular solution model described in the text are shown. (c) The dependence of ln K on $1/T$ (where T is in Kelvin) for several H_2O_t (indicated in the legend) for rhyolitic samples. We have fit the data for all samples with $H_2O_t < 2.5\%$ to the function $\ln K = a + b/T$. The best-fit parameters are $a = 1.89$ and $b = -3120$ (i.e., $\Delta H° = 25.9 \pm 0.4$ kJ/mol and $\Delta S° = 15.7 \pm 0.4$ kJ/mol · K).

state enthalpy change for the reaction among melt species when H_2O_t approaches zero, and T is the temperature in Kelvin. Using the algorithm of Albarède and Provost (1977), the best-fit parameters with 2σ errors are: $A = -1.50 \pm 0.07$, $B = 2.87 \pm 0.05$, $C = 8.88 \pm 0.7$, and $D = -4.53 \pm 0.60$. The standard state enthalpy change of the reaction as H_2O_t approaches zero is thus 23.9 ± 0.4 kJ/mol, similar to the values based on the ideal solution approximations described above. The best-fit isotherms from the regular solution fit are shown in Fig. 1b, and they clearly describe the data well. The double-weight solid curves in Fig. 2 are calculated from our regular solution model at 500C and, again, show that the model fits the data well. The trend in the 500C isotherm shown in Fig. 2 follows the patterns described in earlier studies (Stolper, 1982a; Silver and Stolper, 1989; Silver et al., 1990) in that at low H_2O_t concentrations, OH is the dominant H-bearing species. With increasing H_2O_t, the relative concentration of OH decreases, such that at high total water contents, H_2O_m becomes the prevalent hydrous species. The crossover (i.e., the point at which equal amounts of H_2O are dissolved as H_2O_m and as OH) for rhyolitic glasses and melts occurs at 1.7% H_2O_t at 400C and is predicted to occur at 4.3% at 600C and 8.2% at 850C based on extrapolation of the regular solution model. If the ideal solution model by modifying the calibration of Zhang et al. (1997) is applied, the crossover occurs at 1.8% at 400C, 4.7% at 600C, and 9.3% at 850C.

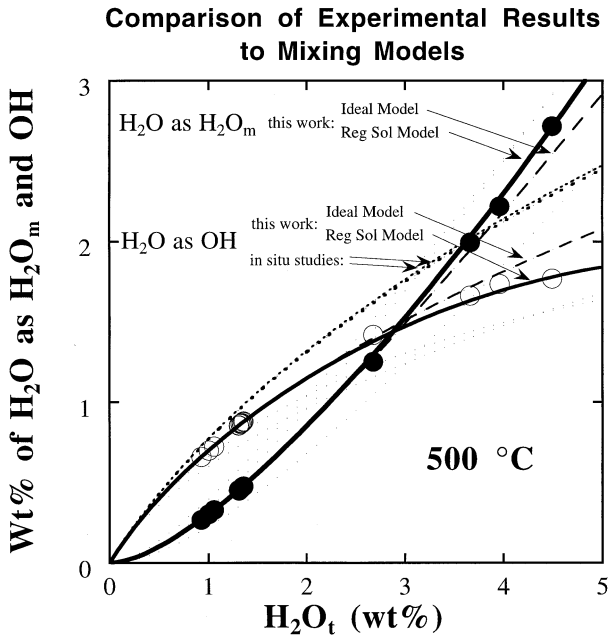

Fig. 2. The equilibrium concentrations of molecular water (solid circles) and hydroxyl species (open circles) in rhyolitic samples held at 500C. Open (OH concentrations) and solid (H_2O_m concentrations) circles are experimental data; errors on experimental data are comparable to or less than the size of the symbols. The solid curves are the species concentrations predicted by the regular solution model and the dashed curves are the species concentrations predicted by the ideal mixing model of this work described in the text. The dotted curves (nearly on top of one another) describe the OH concentrations predicted by the ideal mixing models based on in situ high-temperature measurements of Nowak and Behrens (1995) and Shen and Keppler (1995).

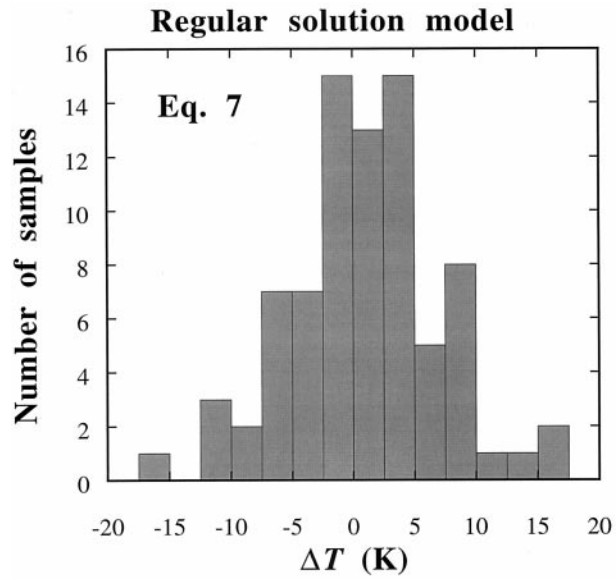

Fig. 3. Histogram showing the distribution of differences between the experimental temperature and the temperature inferred from the measured species concentrations of quenched glasses using the regular solution model (Eqn. 7).

To evaluate further the effect of uncertainties in our experimental data and the accuracy of our regular solution model, Fig. 3 shows in histogram form the difference for each equilibrium experiment in Table 2 between the experimental temperature and the predicted temperature based on the measured H_2O_m and OH and our solution model. Based on the figure, the distribution of errors is roughly Gaussian. The average error is zero, the maximum absolute error in reproducing the temperature is 16C, and twice the standard deviation for the error distribution is 12C. That is, the 2σ uncertainty in reproducing the experimental temperature using Eqn. 7 is 12C. This signifies that even at H_2O_t as low as 0.45% (and H_2O_m as low as 0.08%), the FTIR analyses are accurate enough to predict experimental temperature to within 16C. The accuracy in retrieving experimental temperatures is similar if the ideal solution model is used.

Figure 4 shows the model OH isotherms based on the regular solution fit at 400, 600, 850, and 1200C. An important feature of the results presented in this paper (and their extrapolation to higher H_2O_m and temperature based on the regular solution model) is that the concentration of the hydroxyl species does not fully level off with increasing water content at 400 to 600C with up to about 5% total water content. This result differs from those that predicted that hydroxyl concentrations level off at ~3.5% H_2O_t in rhyolitic glass at 400C (Stolper, 1989) or at ~5.8% H_2O_t ($X_{H_2O_t} \approx 0.1$) in rhyolitic, albitic, orthoclasic, the anorthite–silica eutectic, the anorthite–silica–wollastonite eutectic, and a Na, Zn-rich silicate melt at ≥850C (Silver et al., 1990; Bartholomew et al., 1980). Our analysis supports the interpretation of Dingwell and Webb (1990) that the more extreme leveling off of hydroxyl concentrations observed previously in silicate glasses reflected changes in speciation that occurred on quenching at high water contents rather than a property of melts at high temperature. However, the progressive increase in H_2O_m/OH ratio with increasing H_2O_t and the concave downward trend of hydroxyl concentration (and the concave upward trend of molecular water contents) versus total water content that were the main emphases of these earlier studies remain qualitatively valid descriptions of the behavior of water in silicate melts.

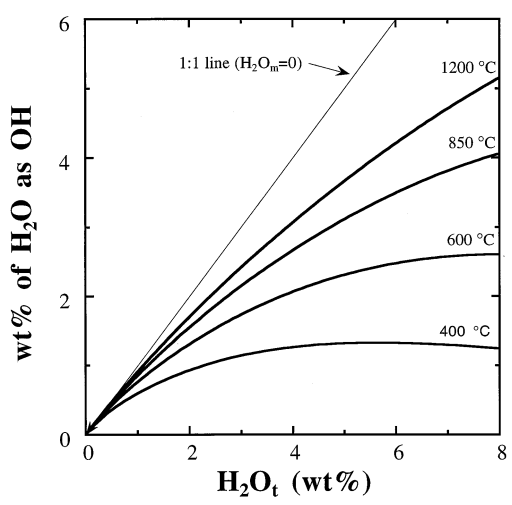

Fig. 4. Predicted isotherms for OH concentration vs. H_2O_t in rhyolite for T = 400, 600, 850, and 1200C using Eqn. 7.

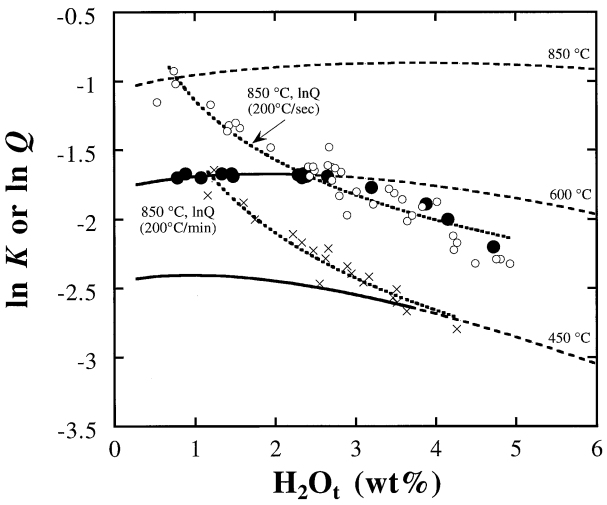

Fig. 5. The measured speciation of water in rhyolitic samples quenched from 600C (this work) and from 850C determined by Silver et al. (1990). Solid circles: rapid quench (~200C/s) from 600C; open circles: rapid quench from 850C; crosses: slow quench (~200C/min) from 850C. Dashed curves show calculated speciation at 850, 600, and 450C using the regular solution model described in the text. Solid curves show calculated speciation from the regular solution model where the model is constrained by the data. Dotted curves are fits to the data of Silver et al. (1990) and define the upper limits of ln K that can be preserved on quenches of ~200C/s (dashed curve) and ~200C/min (dotted curve): $\ln Q_{(\text{rapid quench})} = -1.13–1.44 \ln (H_2O_t)$; $\ln Q_{(\text{slow quench})} = -1.54–1.86 \ln (H_2O_t)$.

3.3. Comparison with Previous Data and Models

Stolper (1989) held natural rhyolitic samples with low H_2O_t at temperatures ranging from 400 to 900C. The data on samples equilibrated at temperatures below 600C from Stolper (1989) are in good agreement with this study, but are more scattered (the average deviation from the model is 23C, the maximum absolute difference is 90C, and 2σ is 62C). We attribute this to the availability for this work of the Nicolet 60SX FTIR spectrophotometer (instead of a Cary 17 spectrophotometer) and our continuing efforts to improve the precision of our measurements over the years. The regular solution fit of Stolper (1989) incorporated data from glasses rapidly quenched from 850C (Silver et al., 1990) that we now know to have been influenced by quenching (Zhang et al., 1991, 1995, and below) and is superseded by the regular solution fit presented here. The regular solution models of Ihinger (1991) and Zhang et al. (1991) were updated by the work of Zhang et al. (1997) using the new calibration. The model of Zhang et al. (1997) is based on preliminary results from this study and is similar to the model presented here, which incorporates additional experimental data for glasses with higher H_2O_t.

Figure 5 shows the speciation data collected by Silver et al. (1990) on a series of water-saturated rhyolitic samples. Their study included samples quenched from 850C both rapidly (in the same apparatus used for the high-pressure experiments of this study) and slowly (by blasting the cold-seal bomb in air to provide quenches at ~200C/min). Each series of experiments shows a well-defined trend in Fig. 5 falling below the 850C isotherm based on extrapolation of the regular solution model presented here. Based either on the analysis of Dingwell and Webb (1990) or on the time scales required to preserve speciation given by Zhang et al. (1995), neither data set would be expected to have preserved on quenching the high-temperature speciation of the experimental temperature. The experiments from this study held at 600C are also plotted in Fig. 5 (solid symbols). The samples with less than 2.5% H_2O_t plot on the 600C isotherm, whereas those with greater than 2.5% H_2O_t fall below the isotherm. This again is consistent with the analysis of Zhang et al. (1995), where at quench rates of 200C/s, samples with less than 2.0% H_2O_t are expected to preserve their speciation on quench from 600C, whereas those with greater than ~2.5% H_2O_t are predicted to reequilibrate on quench from this temperature. Note that the samples with greater than ~2.5% H_2O_t record similar species concentrations to those recorded in glasses with equivalent H_2O_t quenched from 850C in rapid-quench, cold-seal pressure vessels (Silver et al., 1990); i.e., the quenched speciation is independent of the experimental (or peak) temperature as long as the latter is sufficiently high.

Two recent studies have demonstrated that IR measurements can be made on melts in situ at elevated pressures and temperatures (Nowak and Behrens, 1995; Shen and Keppler, 1995). Compared to our results, these in situ studies suggest that significantly higher OH concentrations are present in silicate melt of any given H_2O_t (e.g., about 20% more OH at 3% H_2O_t; see comparisons in Fig. 2). In addition, as noted above, their results suggest a stronger temperature dependence to speciation, manifested by values of ΔH° ~20% to 40% higher than those indicated by our results. There are two possible explanations for these differences.

The first explanation is that the Fe-, Ca-free, lower silica compositions used in their studies may enhance the reaction of water molecules with the silicate network, resulting in higher OH contents at a given H_2O_t. Our preliminary results on a similar haplogranite composition (Q3) corroborate this suggestion. Note that the results for Q3 in Table 2 show at 500 and 475C, respectively, $\ln K = -2.04$ and -2.19 for 3.3% and 3.4% H_2O_t; i.e., at these temperatures, the glasses of haplogranitic composition show OH enrichments of 5% to 10% relative to the concentrations predicted by the regular solution model for rhyolitic compositions.

A second explanation is that the molar absorptivities for H_2O_m and OH change with measurement temperature, contrary to the assumption of both of the in situ high-temperature studies. If this was the case, it would undermine the quantitative determinations of species concentrations at high temperature. In support of this possibility, Zhang and Behrens (1998) demonstrated that in situ measurements on rhyolitic samples at temperatures below 400C appear to record anomalous changes in species concentrations with changing temperature, but that on closer inspection, these changes are better explained by variations in molar absorptivities. They compared two samples for the relative variation of the OH band intensity with temperature. One sample had negligible H_2O_m ($H_2O_t = 0.18\%$) while the other had significant H_2O_m ($H_2O_t = 0.76\%$). When in situ measurements were made from 25 to 400C, the intensity of the OH band at 4520 cm^{-1} in both samples increased by the same percentage. If some sort of equilibrium reaction was responsible for the OH band increase, the relative variation of the intensity of the OH band would be different: the low H_2O_t

sample had insignificant H_2O_m and hence the OH band increase would be insignificant, whereas the higher water sample had significant H_2O_m and hence the OH band increase would be significant. The fact that the OH band intensity in both samples increases by the same percentage is best explained by the temperature dependence of the molar absorptivity. With the erroneous assumption of temperature-independent molar absorptivities, these changes would be mistakenly interpreted as reflecting a change in species concentration. Zhang and Behrens (1998) and Behrens et al. (1998) also demonstrate that the degree to which the molar absorptivities vary with temperature depends on how the baseline is fit (curved vs. straight-line fits). A straight-line fit to the baseline (as used by Nowak and Behrens, 1995; the fit by Shen and Keppler, 1995, is not specified), results in a greater temperature dependence of the molar absorptivities than when the baseline is fit by a flexicurve.

The temperature dependence of molar absorptivities is supported also by recent results of Grzechnik and McMillan (1998) who investigate the temperature dependence of the absorption at 3680 cm^{-1} in SiO_2 glass. There are changes in band characteristics: a 12% decrease in band width, a 4% decrease in peak height, and a 36% decrease in the integrated absorbance was observed for in situ spectra of samples with 1200 ppm H_2O_t on heating from room temperature to the glass transition temperature at 1300 K. We conclude that although in situ techniques hold much promise for future speciation studies in hydrous silicate melt, the effects of temperature on the molar absorptivities at 5230 and 4520 cm^{-1} will need to be quantified before accurate concentrations of H_2O_m and OH and their temperature dependence can be determined with these techniques and compared with confidence to our results.

3.4. Prediction of Species Concentrations and Apparent Equilibrium Temperature

Our results provide a direct determination of H_2O_m and OH concentrations as functions of temperature and H_2O_t in rhyolitic melts and glasses at low temperatures and H_2O_t, and these measurements can be extrapolated to higher temperatures and H_2O_t using the regular solution formulation. The ability to model species concentrations in this way is essential to a quantitative understanding of the effect of dissolved H_2O_t on the thermodynamic properties of silicate melts (Ghiorso and Sack, 1995), on crystal–liquid phase equilibria (Kushiro, 1975; Stolper, 1982b), on the viscosity of silicate melts (Shaw, 1972; Stolper, 1982a), on the diffusion of water in silicate glasses and melts (Zhang and Stolper, 1991; Zhang et al., 1991), and on the nucleation and crystal growth rates in silicate melts (Davis et al., 1997; Davis and Ihinger, 1997). As discussed above, measurement and prediction of H_2O_m and OH concentrations to higher water contents and in situ at higher temperatures will require improvements in determinations of molar absorptivities for H_2O_m and OH. Although such improvements will no doubt result in changes in the values of A, B, C, and D in Eqn. 7, sufficient data have accumulated independently from several labs that we can state with confidence that the overall trends in species concentrations with total water content and temperature shown here are robust and will not be affected by such changes.

One application of our results is to predict the "apparent" equilibration temperature (T_{ae}, Zhang, 1994) of a naturally cooled, hydrous glass. As shown above (Fig. 3), experimental temperatures can be accurately reproduced from the measured species concentrations with a 2σ uncertainty of 12C by using Eqn. 7, provided the sample is in the region of parameter space (i.e., cooling rate and H_2O_t) that allows high-temperature speciation to be preserved on quenching. It is important to emphasize that this accuracy in retrieving the experimental temperature and hence in predicting T_{ae} is independent of the accuracy of the molar absorptivities; i.e., as long as the molar absorptivities of Zhang et al. (1997) are used, Eqn. 7 with the constants we obtained *accurately* predicts T_{ae}. However, because the values of molar absorptivities may continue to improve in the future, it may be more useful to relate directly the intensities of the 5230 and 4520 cm^{-1} bands and the experimental temperature:

$$\ln \frac{A_{452}^2}{A_{523}} = a_0 + \frac{1000}{T}(b_0 + b_1 A_{523} + b_2 A_{452}), \qquad (8)$$

where A_{523} and A_{452} are the absorbances (peak heights) for the 5230 and 4520 cm^{-1} bands per mm sample thickness. The above formula is obtained by analogy to the regular solution model (Eqn. 7). The best-fit parameters (with 2σ uncertainties) are: $a_0 = 2.48 \pm 0.13$, $b_0 = -2.66 \pm 0.09$, $b_1 = -0.09 \pm 0.15$, $b_2 = -1.08 \pm 0.30$. Eqn. 8 is independent of any knowledge of the molar absorptivities and the actual H_2O_m and OH concentrations, and it can reproduce experimental temperature with a 2σ uncertainty of 13C (similar to the reproducibility of Eqn. 7 shown in Fig. 3) directly from measured absorbances; i.e., future improvements in molar absorptivities will only change parameters in Eqn. 7, not in Eqn. 8.

3.5. Conditions Involving Species Reequilibration on Quench: Inaccessible Regions of Temperature and H_2O_t in Preserving Equilibrium Speciation

Our results confirm the predictions of Dingwell and Webb (1990) and the results of Zhang et al. (1995, 1997b) that for a given H_2O_t and cooling rate, there is a temperature above which samples cannot be quenched without the speciation changing on cooling. Likewise, for a given temperature, there is a water content above which speciation cannot be preserved for any realistic cooling rates. Thus, for a given cooling rate, there will be a curve of negative slope on a ln Q vs. H_2O_t diagram defining the limiting conditions for preserving speciation on quench; i.e., high-temperature speciation can only be preserved for temperatures and water contents below this curve. The limiting curve will depend on cooling rate, moving up on the ln Q vs. H_2O_t diagram for faster quenching rates. This is illustrated in Figure 5, in which the species concentrations of glasses quenched from 850C in rapid-quench cold-seal apparatus (200C/s; Silver et al., 1990) and data from this study on samples with >2.5% H_2O_t quenched at similar cooling rates from 600C define such a curve and are compared with the isotherms from this study. Glasses quenched at this rate from conditions (i.e., temperatures and water contents) above the limiting curve will change speciation on quenching (OH will convert to H_2O_m and anhydrous oxygen ions; i.e., Q will decrease), and the final speciation will lie on the curve; glasses

quenched at this rate from conditions below the limiting curve will not undergo significant changes in speciation on quenching. Also shown are speciation results for glasses quenched from 850C at a slower rate (200C/m; Silver et al., 1990). These results also fall on a curve, lower than the one for the faster cooling rate by ~0.5 ln Q units (i.e., relaxation of the high-temperature speciation on quenching proceeds to lower temperature, freezing in a lower value of Q for the same H_2O_t), that defines the limiting conditions for preserving high-temperature speciation for this cooling rate. The dependence of the quenched-in speciation on cooling rate and H_2O_t can provide insights into the relaxation behavior of hydrous rhyolite (Dingwell and Webb, 1990) and can be inverted to determine cooling rates of natural hydrous obsidians if the thermal history is one of simple monotonic cooling (Ihinger, 1991; Newman et al., 1993; Zhang et al., 1995; Zhang et al., 1997b). The distribution of hydrous species in natural samples can thus, in principle, serve as a geospeedometer that can be compared to other estimates of cooling rates (Wilding et al., 1995; Stevenson et al., 1995).

4. CONCLUSIONS

Concentrations of water molecules and hydroxyl groups have been measured at room temperature in rhyolitic glasses with 0.5% to 5.0% H_2O_t. These glasses were cooled at ~10^2C/s after having been held at 400 to 600C, for sufficient time for the equilibrium distribution of species to have been reached.

The speciation data at $H_2O_t < 2.5\%$ can be described by an ideal solution model. The speciation at higher H_2O_t is less certain owing to the possible uncertainty in the IR calibration. One way to describe all the speciation data is by a regular solution model with:

$$\ln K = (1.50 \pm 0.07) - \frac{1}{T}[(2870 \pm 50) + (8880 \pm 700)X_{H_2O_m} - (4530 \pm 600)X_{OH}],$$

where the uncertainties are at the 2σ level. This equation can be extrapolated to predict high-temperature species concentrations as a function of temperature and H_2O_t and to predict experimental or apparent equilibrium temperatures of natural or synthetic quenched rhyolitic glasses.

At a given quench rate, there is a temperature vs. H_2O_t curve above which the species concentrations cannot be preserved on quenching and below which the species concentrations can be preserved. With a quench rate of ~200C/s, species concentrations at 850C can be preserved for $H_2O_t < 0.6\%$ but cannot be preserved for $H_2O_t > 0.8\%$.

Acknowledgments—We thank Dr. D. Hamilton and Dr. T. Stanton for providing some of the starting glasses. Reviews by James Blencoe, Marcus Nowak, Hans Keppler, and Don Dingwell contributed to the manuscript. This research is supported by NSF grants EAR-92-19899 (to E.M.S.), EAR-93-04548 (to P.D.I.), and EAR-9458368 (to Y.Z.), and DOE grant DEFG03-85ER13445 (to E.M.S.). Division of Geological and Planetary Sciences Contribution no. 5592.

REFERENCES

Albarède F. and Provost A. (1977) Petrological and geochemical mass-balance equations: An algorithm for least-squares fitting and general error analysis. *Comput. Geosci.* **3,** 309–326.

Bartholomew R. F., Butler B. L., Hoover H. L., and Wu C. K. (1980) Infrared spectra of a water-containing glass. *J. Am. Ceram. Soc.* **63,** 481–485.

Behrens H. and Nowak M. (1997) The mechanism of water dissolution in polymerized silicate melts. *Contrib. Mineral. Petrol.* **126,** 377–385.

Behrens H., Withers A., and Zhang Y. (1998) In situ IR spectroscopy on hydrous albitic and rhyolitic glasses and its implications for water speciation and water reactions in silicate glasses and melts. *Goldschmidt Conf.*; *Mineral. Mag.* **62A,** 139–140.

Burnham C. W. (1967) Hydrothermal fluids at the magmatic stage. In *Geochemistry of Hydrothermal Ore Deposits* (ed. H. L. Barnes), pp. 34–76. Holt, Rinehart and Winston.

Burnham C. W. (1975) Water and magmas; a mixing model. *Geochim. Cosmochim. Acta* **39,** 1077–1084.

Davis M. J. and Ihinger P. D. (1997) The influence of water on crystal growth rates in silicate melt. *EOS Fall Meeting,* EOS Trans. AGU **78,** F834 (suppl.).

Davis M. J., Ihinger P. D., and Lasaga A. C. (1997) The influence of water on nucleation kinetics in silicate melt. *J. Non-Cryst. Solids* **219,** 62–69.

Dingwell D. B. (1993) Experimental strategies for the investigation of low temperature properties in granitic and pegmatitic melts. *Chem. Geol.* **108,** 19–30.

Dingwell D. B. and Webb S. L. (1990) Relaxation in silicate melts. *Eur. J. Mineral.* **2,** 427–449.

Dingwell D. B., Romano C., and Hess K.-U. (1996) The effect of water on the viscosity of a haplogranitic melt under P-T-X conditions relevant to silicic volcanism. *Contrib. Mineral. Petrol.* **124,** 19–28.

Doremus R. H. (1994) *Glass Science*. Wiley.

Ghiorso M. S. and Sack R. O. (1995) Chemical mass transfer in magmatic processes IV. A revised and internally consistent thermodynamic model for the interpolation and extrapolation of liquid-solid equilibria in magmatic systems at elevated temperatures and pressures. *Contr. Mineral. Petrol.* **119,** 197–212.

Goranson R. W. (1938) Silicate-water systems: phase equilibria in the $NaAlSi_3O_8$–H_2O and $KAlSi_3O_8$–H_2O systems at high temperatures and pressures. *Am. J. Sci.* **35-A,** 71–91.

Grzechnik A. and McMillan P. F. (1998) Temperature dependence of the OH− absorption in SiO_2 glass and melt to 1975 K. *Am. Mineral.* **83,** 331–338.

Ihinger P. D. (1991) An experimental study of the interaction of water with granitic melt. PhD, California Institute of Technology.

Kohn S. C., Dupree R., and Golam Mortuza M. (1992) The interaction between water and aluminosilicate magmas. *Chem. Geol.* **96,** 399–409.

Kohn S. C., Dupree R., and Smith M. E. (1989) A multinuclear magnetic resonance study of the structure of hydrous albite glasses. *Geochim. Cosmochim. Acta* **53,** 2925–2935.

Kushiro I. (1969) The system forsterite-diopside-silica with and without water at high pressures. *Am. J. Sci.* **267-A,** 269–294.

Kushiro I. (1975) On the nature of silicate melt and its significance in magma genesis: Regularities in the shift of liquidus boundaries involving olivine, pyroxene, and silica minerals. *Am. J. Sci.* **275,** 411–431.

McMillan P. F., Wolf G. H., and Poe B. T. (1992) Vibrational spectroscopy of silicate liquids and glasses. *Chem. Geol.* **96,** 351–366.

Mysen B. (1993) Peralkalinity, Al–Si substitution, and solubility mechanisms of H_2O in aluminosilicate melts. *J. Petrol.* **33,** 347–375.

Mysen B. O. and Virgo D. (1986) Volatiles in silicate melts at high pressure and temperature. 1. Interaction between OH groups and Si^{4+}, Al^{3+}, Ca^{2+}, Na^+ and H^+. *Chem. Geol.* **57,** 303–331.

Newman S., Epstein S., and Stolper E. (1988) Water, carbon dioxide, and hydrogen isotopes in glasses from the ca. 1340 A.D. eruption of the Mono Craters, California: Constraints on degassing phenomena and initial volatile content. *J. Volcanol. Geotherm. Res.* **35,** 75–96.

Newman S., Stolper E. M., and Epstein S. (1986) Measurement of

water in rhyolitic glasses: Calibration of an infrared spectroscopic technique. *Am. Mineral.* **71,** 1527–1541.

Newman S., Blouke K., Bashir N., Ihinger P., and Stolper E. (1993) Cooling of rhyolitic volcanics-evidence from melt inclusions. *GSA Annual Mtg. Suppl.,* **25,** Vol. p. A-43 (abstr.).

Nowak M. and Behrens H. (1995) The speciation of water in haplogranitic glasses and melts determined by in situ near-infrared spectroscopy. *Geochim. Cosmochim. Acta* **59,** 3445–3450.

Romano C., Dingwell D. B., and Behrens H. (1995) The temperature dependence of the speciation of water in $NaAlSi_3O_8$–$KAlSi_3O_8$ melts: An application of fictive temperatures derived from synthetic fluid-inclusions. *Contrib. Mineral. Petrol.* **122,** 1–10.

Schulze F., Behrens H., Holtz F., Roux J., and Johannes W. (1996) The influence of H_2O on the viscosity of a haplogranitic melt. *Am. Mineral.* **81,** 1155–1165.

Shaw H. R. (1963) Obsidian-H_2O viscosities at 1000 and 2000 bar in the temperature range 700° to 900C. *J. Geophys. Res.* **68,** 6337–6343.

Shaw H. R. (1972) Viscosities of magmatic silicate liquids: An empirical method of prediction. *Am. J. Sci.* **272,** 870–893.

Shen A. and Keppler H. (1995) Infrared spectroscopy of hydrous silicate melts to 1000C and 10 kbar: Direct observation of H_2O speciation in a diamond-anvil cell. *Am. Mineral.* **80,** 1335–1338.

Sieh K. and Bursik M. (1986) Most recent eruption of the Mono Craters, eastern central California. *J. Geophys. Res.* **91,** 12,539–12,571.

Silver L. A. and Stolper E. M. (1985) A thermodynamic model for hydrous silicate melts. *J. Geol.* **93,** 161–177.

Silver L. A. and Stolper E. M. (1989) Water in albitic glasses. *J. Petrol.* **30,** 667–709.

Silver L. A., Ihinger P. D., and Stolper E. M. (1990) The influence of bulk composition on the speciation of water in silicate glasses. *Contr. Mineral. Petrol.* **104,** 142–162.

Stanton T. R. (1989) High pressure, isotopic studies of the water diffusion mechanism in silicate melts and glasses. PhD dissertation, Arizona State University.

Stevenson R. J., Bagdassarov N. S., Dingwell D. B., and Romano C. (1998) The influence of trace amounts of water on the viscosity of rhyolites. *Bull. Volcanol.* **60,** 89–97.

Stevenson R. J., Dingwell D. B., Webb S. L., and Bagdassarov N. S. (1995) The equivalence of enthalpy and shear stress relaxation in rhyolitic obsidians and quantification of the liquid–glass transition in volcanic processes. *J. Volcanol. Geotherm. Res.* **68,** 297–306.

Stolper E. M. (1982a) Water in silicate glasses: An infrared spectroscopic study. *Contr. Mineral. Petrol.* **81,** 1–17.

Stolper E. M. (1982b) The speciation of water in silicate melts. *Geochim. Cosmochim. Acta* **46,** 2609–2620.

Stolper E. M. (1989) The temperature dependence of the speciation of water in rhyolitic melts and glasses. *Am. Mineral.* **74,** 1247–1257.

Sykes D. and Kubicki J. D. (1993) A model for H_2O solubility mechanisms in albite melts from infrared spectroscopy and molecular orbital calculations. *Geochim. Cosmochim. Acta* **57,** 1039–1052.

Tuttle O. F. and Bowen N. L. (1958) Origin of granite in the light of experimental studies in the system $NaAlSi_3O_8$–$KAlSi_3O_8$–SiO_2–H_2O. *Geolog. Soc. Am. Memoirs* **74,** 1–153.

Wasserburg G. J. (1957) The effects of H_2O in silicate systems. *J. Geol.* **65,** 15–23.

Watson E. B. (1979) Diffusion of cesium ions in H_2O-saturated granitic melt. *Science* **205,** 1259–1260.

Wilding M. C., Webb S. L., and Dingwell D. B. (1995) Evaluation of a relaxation geospeedometer for volcanic glass. *Chem. Geol.* **125,** 137–148.

Wyllie P. J. (1979) Magmas and volatile components. *Am. Mineral.* **64,** 469–500.

Zhang Y. (1993) Pressure dependence of the speciation of water in rhyolitic glasses. *EOS* **74,** 631 (abstr.).

Zhang Y. (1994) Reaction kinetics, geospeedometry, and relaxation theory. *Earth Planet. Sci. Lett.* **122,** 373–391.

Zhang Y. and Behrens H. (1998) Resolving the controversy between quenched and in situ H_2O speciation in silicate melts and glasses. *Western Pacific AGU Meeting, Eos* **79,** W123–W124.

Zhang Y. and Stolper E. M. (1991) Diffusion of water in a basaltic melt. *Nature* **351,** 306–309.

Zhang Y., Jenkins J., and Xu Z. (1997b) Kinetics of the reaction $H_2O + O = 2OH$ in rhyolitic glasses upon cooling: Geospeedometry and comparison with glass transition. *Geochim. Cosmochim. Acta* **61,** 2167–2173.

Zhang Y., Stolper E. M., and Ihinger P. D. (1995) Kinetics of reaction $H_2O + O = 2OH$ in rhyolitic glasses: Preliminary results. *Am. Mineral.* **80,** 593–612.

Zhang Y., Stolper E. M., and Wasserburg G. J. (1991) Diffusion of water in rhyolitic glasses. *Geochim. Cosmochim. Acta* **55,** 441–456.

Zhang Y., Belcher R., Ihinger P. D., Wang L., Xu Z., and Newman S. (1997) New calibration of infrared measurement of dissolved water in rhyolitic glasses. *Geochim. Cosmochim. Acta* **61,** 3089–3100.